Synchrotron X-ray diffraction study of double perovskites Sr_2RNbO_6 (R = Sm, Gd, Dy, Ho, Y, Tm, and Lu)

W. Wong-Ng,[1,a] J. A. Kaduk,[2] S. H. Lapidus,[3] L. Ribaud,[3] and S. P. Diwanji[1]
[1]*Materials Measurement Science Division, National Institute of Standards AND Technology, Gaithersburg, Maryland 20899*
[2]*Department of Chemical Science, Illinois Institute of Technology, Chicago, Illinois 60616*
[3]*Advanced Photon Source, Argonne National Laboratory, Argonne, Illinois 60439*

(Received 2 March 2018; accepted 28 June 2018)

A series of double-perovskite oxides, Sr_2RNbO_6 (R = Sm, Gd, Dy, Ho, Y, Tm, and Lu) were prepared and their crystal structure and powder diffraction reference patterns were determined using the Rietveld analysis technique. The crystal structure of each of the Sr_2RNbO_6 phase is reported in this paper. The R = Gd, Ho, and Lu samples were studied using synchrotron radiation, while R = Sm, Dy, Y, and Tm samples were studied using laboratory X-ray diffraction. Members of Sr_2RNbO_6 are monoclinic with a space group of $P2_1/n$ and are isostructural with each other. Following the trend of "lanthanide contraction", from R = Sm to Lu, the lattice parameters "a" of these compounds decreases from 5.84672(10) to 5.78100(3) Å, b from 5.93192(13) to 5.80977(3) Å, c from 8.3142(2) to 8.18957(5) Å, and V decreases from 288.355(11) to 275.057(2) Å^3. In this double-perovskite series, the R^{3+} and Nb^{5+} ions are structurally ordered. The average Nb–O bond length is nearly constant, while the average R–O bond length decreases with the decreasing ionic radius of R^{3+}. Powder diffraction patterns for these compounds have been submitted to the Powder Diffraction File (PDF). © *2018 International Centre for Diffraction Data.* [doi:10.1017/S0885715618000593]

Key words: Sr_2RNbO_6 (R = Sm, Gd, Dy, Ho, Y, Tm, and Lu), double perovskites, synchrotron X-ray studies, X-ray diffraction patterns and structures

I. INTRODUCTION

The efficiency and performance of thermoelectric energy conversion or cooling is related to the dimensionless figure of merit (ZT) of the thermoelectric (TE) materials, given by $ZT = S^2T/\rho\kappa$, where T is the absolute temperature, S is the Seebeck coefficient or thermoelectric power, ρ is the electrical resistivity, and k is the thermal conductivity (Nolas *et al*., 2001). For high-temperature waste heat conversion applications, low-dimensional layered oxides have been found to have potential high efficiency. Examples of these oxides include "natural superlattice" oxides such as $NaCo_2O_4$ (Terasaki *et al*., 1997), $Ca_3Co_4O_9$ (Masset *et al*., 2000; Li *et al*., 2001; Minami *et al*., 2002; Grebille *et al*., 2004; Otani *et al*., 2007; Wong-Ng *et al*., 2007; 2010), $Bi_2Sr_2Co_2O_x$ (Wang *et al*., 2009), (Bi.Pb) CuSeO (Wong-Ng *et al*., 2016), and (Bi.A)CuSeO (A = Ba, Sr, and Ca) (Wong-Ng *et al*., 2017). The search for oxide compounds with superior thermoelectric properties continues.

Perovskite materials such as $La_{1-x}A_xCoO_3$ (A = Ca, Sr) (Sehlin *et al*., 1995; Wang *et al*., 2010) and $RCoO_3$ (Moon *et al*., 2001) have demonstrated large Seebeck coefficient and low resistivity. These compounds have been reported to have long-range magnetic ordering at low temperature, and is frustrated by the geometry of the crystalline lattice, a situation known as geometrical magnetic frustration (Henmi and Hinatsu, 1999; Karunadasa *et al*., 2003). Besides cobaltates, niobate compounds such as $(Sr.Ba)_6Nb_{10}O_{30}$ have also been reported to possess good thermoelectric properties (Chan *et al*., 2017).

Sr_2RNbO_6 is a series of double-perovskite niobates that have potential for thermoelectric applications as well. Since X-ray diffraction is a non-destructive technique for phase identification, X-ray diffraction patterns are especially important for phase characterization. Therefore, the main goal of this investigation is to determine the crystal structure, crystal chemistry, and experimental powder X-ray diffraction patterns for the niobate series Sr_2RNbO_6 (R = Sm, Gd, Dy, Ho, Y, Tm, and Lu), and to make these patterns available in the Powder Diffraction File (PDF) (McMurdie *et al*., 1986; Wong-Ng *et al*., 2001; PDF 2018).

II. EXPERIMENTAL DETAILS

A. Sample preparation

Samples were prepared in two groups (R = Gd, Ho, and Lu as the first group and R = Sm, Dy, Y, and Tm as the second group). All samples were prepared by heating a stoichiometric mixture of $SrCO_3$, R_2O_3, and Nb_2O_5 in air. Sm_2O_3 was first heat-treated at 550 °C overnight prior to use to ensure the absence of carbonates and hydroxides. Samples were weighed out, well-mixed and calcined overnight at 750 °C, 950 °C for 2 days, 1200 °C for 2 days, and finally at 1250 °C for another 2 days, with intermediate grindings. During each heat treatment, the samples were furnace cooled. The phase purity of the samples was established by powder X-ray diffraction. Patterns were taken at 300 K.

[a]Author to whom correspondence should be addressed. Electronic mail: winnie.wong-ng@nist.gov

https://doi.org/10.1017/S0885715618000593 Published online by Cambridge University Press

TABLE I. Results of Rietveld refinements for Sr_2RNbO_6 (R = Sm, Gd, Dy, Ho, Y, Tm, and Lu).

R	Sm	Gd	Dy	Ho	Y	Tm	Lu
BV r_0, Å	2.088	2.065	2.036	2.023	2.014	2.000	1.971
Space group	$P2_1/n$	$P2_1/n$	$P2_1/n$	$P2_1/n$	$P2_1/n$	$P2_1/n$	$P2_1/n$
R_{wp}	0.1544	0.1776	0.1186	0.1658	0.1480	0.0848	0.1450
R_p	0.1202	0.1366	0.0893	0.1303	0.1016	0.0627	0.1188
χ^2	3.643	1.983	4.572	2.055	6.262	3.612	2.070
R(F)	0.0832	0.0868	0.1552	0.0997	0.0639	0.0475	0.1078
R_2O_3 cubic, wt%	–	0.22(6)	1.6(1)	0.43(5)	1.2(1)	1.4(1)	–
Monoclinic, wt%	–	1.2(1)	–	–	–	–	–
R_3NbO_7, wt%	–	0.28(7)	–	1.74(4)	–	–	–

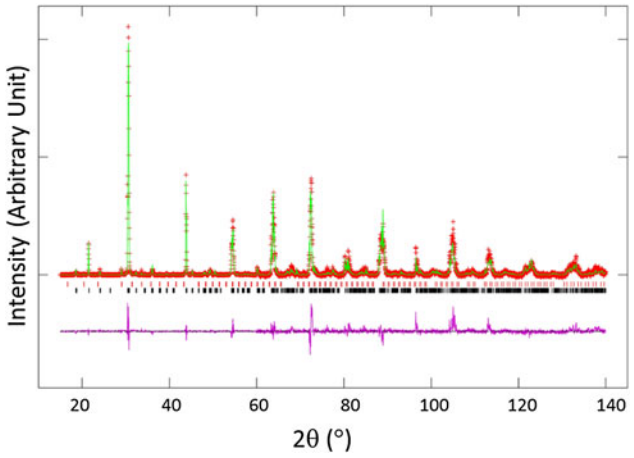


Figure 1. Observed (crosses), calculated (solid line), and difference XRD pattern (bottom) for Sr_2DyNbO_6 by Rietveld analysis technique. The observed data are indicated by crosses and the calculated profile is the solid line. The vertical lines below the profiles mark the positions of all possible Bragg reflections. The difference pattern is plotted at the same scale as the other calculated peak position.

B. X-ray Rietveld refinements and powder reference patterns

For R = Gd, Ho, and Lu, powder patterns were collected from rotated 0.7 mm capillary specimens at the MR-CAT 11-ID beamline at the Advanced Photon Source (APS) at the Argonne National Laboratory, using a wavelength of 0.49516 Å. High-resolution synchrotron X-ray powder diffraction data were collected using beamline 11-BM at the APS, Argonne National Laboratory. Discrete detectors covered a final angular range from 0 to 50°, with data points collected every 0.001° in 2θ at a scan speed of 0.01° s^{-1}. The instrumental optics of 11-BM incorporate two platinum-striped mirrors and a double-crystal Si (111) monochromator, where the second crystal has an adjustable sagittal bend (Wang *et al.*, 2008). The diffractometer is controlled via EPICS (Dalesio *et al.*, 1994). A vertical Huber 480 goniometer positions 12 perfect Si (111) analyzers and 12 Oxford-Danfysik $LaCl_3$ scintillators, with a spacing of 2° in 2θ (Lee *et al.*, 2008). Capillary samples are mounted by a robotic arm and spun at ≈90 Hz. Data are normalized to incident flux and collected while continually scanning the diffractometer 2θ arm. A mixture of National Institute of Standard and Technology standard reference materials, Si (SRM™ 640c) and Al_2O_3 (SRM™ 676), is used to calibrate the instrument, where the Si lattice constant determines the wavelength for each detector. Corrections are applied for detector sensitivity, 2θ offset, and small detector wavelength differences, before merging the data into a single set of intensities evenly spaced in 2θ. For R = Sm, Dy, Y, and Tm, the Sr_2RNbO_6 patterns were measured from flat plate specimens using Cu$K\alpha$ radiation on a Scintag PAD V diffractometer equipped with an Ortec intrinsic Ge detector.

The Rietveld refinement technique (Rietveld, 1969; Larson and von Dreele, 2004) with the software suite GSAS (Larson and Von Dreele, 2004) was used to determine the structure of Sr_2RNbO_6. The structure of the Sr_2EuNbO_6 phase (PDF 4-18-9033) (Huang *et al.*, 1991; PDF, 2018) was used as a model for refinement. Reference patterns were obtained with a Rietveld pattern decomposition

TABLE II. Crystallographic data for Sr_2RNbO_6 (space group: $P2_1/n$) for R = Sm, Gd, Dy, Ho, Y, Tm, and Lu; $r(R^{3+})$ is the Shannon ionic radius (1976) using VI coordination.

		Cell parameters						
R	$r(R^{3+})$	a(Å)	b(Å)	c(Å)	β (°)	V(Å^3)	*s.p.*	D_x g cm^{-3}
Sm	0.958	5.84672(10)	5.93192(13)	8.3142(2)	90.212(2)	288.355(11)	$P2_1/n$	5.93
Eu	0.947	5.844	5.925	8.307	90.22	287.66	$P2_1/n$	5.96 (Maupoey *et al.*, 2012)
Gd	0.938	5.83333(2)	5.91016(2)	8.29095(3)	90.1968(3)	285.837(1)	$P2_1/n$	6.06
Dy	0.912	5.81448(10)	5.87239(10)	8.2534(2)	90.1540(15)	281.810(10)	$P2_1/n$	6.21
Ho	0.901	5.80600(2)	5.85649(2)	8.23730(4)	90.1529(4)	280.090(2)	$P2_1/n$	6.27
Y	0.900	5.80787(8)	5.85753(9)	8.23820(14)	90.1579(11	280.261(6)	$P2_1/n$	5.37
Tm	0.880	5.79447(8)	5.83089(7)	8.21240(11)	90.1466(10)	277.471(6)	$P2_1/n$	6.38
Lu	0.861	5.78100(3)	5.80977(3)	8.18957(5)	90.1163(5)	275.057(2)	$P2_1/n$	6.51

https://doi.org/10.1017/S0885715618000593 Published online by Cambridge University Press

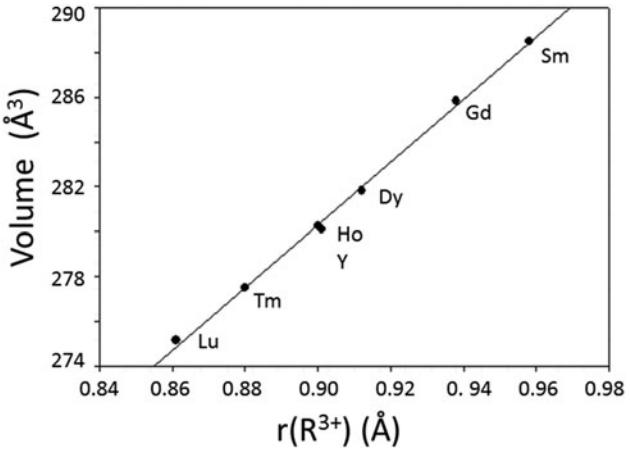


Figure 2. Plot of unit-cell volume of Sr_2RNbO_6 (R = Sm, Gd, Dy, Ho, Y, Tm, Yb, and Lu vs. $r(R^{3+})$ [where "r" is the Shannon ionic radii (1976)], space group $P2_1/n$.

technique. Using this technique, the reported peak positions were derived from the extracted integrated intensities, and positions calculated from the lattice parameters. When peaks are not resolved at the resolution function, the intensities are summed, and an intensity-weighted d-spacing is reported. They are also corrected for systematic errors both in d-spacing and intensity. In summary, these patterns represent ideal specimen patterns.

C. Bond valence sum (V_b) calculations

The bond valence sum values, V_b, for Sr, R, and Nb were calculated using the Brown–Altermatt empirical expression (Shannon, 1976; Brese and O'Keeffe, 1991; Brown and Altermatt, 1985), and the results are also listed in Table III. The V_b of an atom i is defined as the sum of the bond valences v_{ij} of all the bonds from atoms i to atoms j. The most commonly adopted empirical expression for the bond valence v_{ij} as a function of the interatomic distance d_{ij} is $v_{ij} = \exp[(R_0 - d_{ij})/B]$. The parameter, B, is commonly taken to be a "universal" constant equal to 0.37 Å. The values for the reference distance, R_0: Sr–O 2.118, Nb–O 1.911, Sm–O 2.088, Gd–O 2.065, Dy–O 2.036, Ho–O 2.023, Y–O 2.014, Tm–O 2.000, Lu–O 1.971 (Brown and Altermatt, 1985).

III. RESULTS AND DISCUSSION

The structural details are summarized in Table I and in the supported information (cif files). The trends in lattice parameters (Table I) show that the seven Sr_2RNbO_6 compounds are isostructural, and crystallized in a distorted Ö2a × Ö2a × 2a perovskite superstructure, with a space group of $P2_1/n$.

Table I also gives the refinement residuals for Sr_2RNbO_6 (R = Sm, Gd, Dy, Ho, Y, Tm, and Lu). Figure 1 provides the Rietveld refinement results for Sr_2DyNbO_6 as an example. The observed (crosses), calculated (solid line), and difference XRD patterns (bottom) for Sr_2LuNbO_6, as determined by the Rietveld analysis technique, are shown. The difference pattern is plotted at the same scale as the other patterns up to 60° 2θ. At higher 2θ angles, the scale has been magnified five times. The row of tick marks refers to the calculated peak positions. The refinement residuals mainly reflect

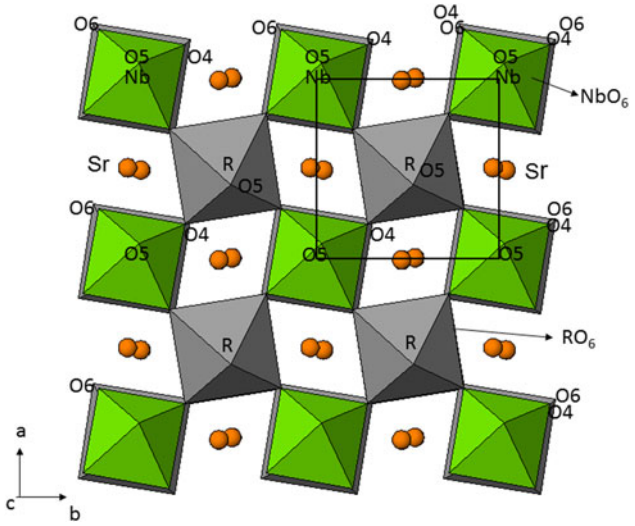


Figure 3. Crystal structure of Sr_2DyNbO_6 at room temperature showing the unit-cell outline and the top view (viewing along c) of B-site octahedra.

variations in the counting times, and the presence of traces of additional impurities.

It is noted that the structure of larger size lanthanide members Sr_2LaNbO_6 (Trunov *et al*., 1983; Huang *et al*., 1991) and Sr_2PrNbO_6 (Trunov *et al*., 1983) is cubic with space group *Fm*-3*m*. The structure transition from cubic to monoclinic $P2_1/n$ for the smaller size Sr_2RSbO_6. Table II lists the lattice parameters and calculated density, D_x, for the $P2_1/c$ Sr_2RSbO_6. It is seen that the lattice parameters a, b, and c for the monoclinic structures all decrease from R = Sm to Lu [5.84672(10) to 5.78100(3) Å, b from 5.93192(13) to 5.80977(3) Å, c from 8.3142(2) to 8.18957(5) Å, and V decreases from 288.355(11) to 275.057(2) Å^3], following the trend of "lanthanide contraction". The calculated density values, D_x, increases as the size of R decreases (5.927–6.508 g cm^{-3}). Figure 2 gives the plot of the unit-cell volumes, V, of Sr_2RNbO_6 vs. Shannon ionic radius of R^{3+} (r_R). The unit-cell volume decreases across the lanthanide series from Sm to Lu, or with the decreasing size of the ionic radius (Shannon, 1976) (lanthanide contraction) of the metal ion at

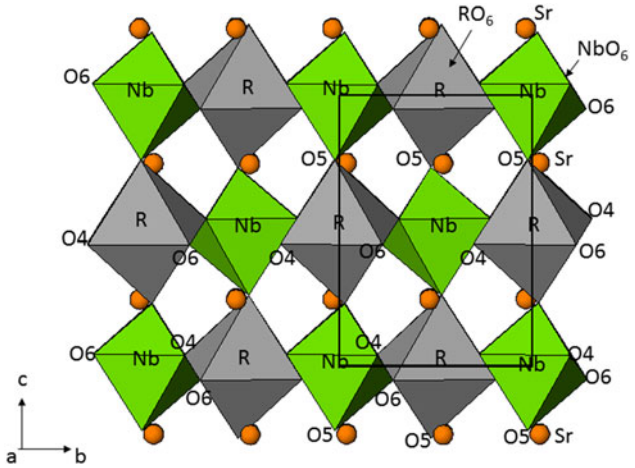


Figure 4. Crystal structure of Sr_2DyNbO_6 at room temperature showing the unit-cell outline and the view along a.

https://doi.org/10.1017/S0885715618000593 Published online by Cambridge University Press

TABLE III. Atomic coordinates and isotropic displacement factors for Sr_2RNbO_6 (R = Sm, Gd, Dy, Ho, Y, Tm, and Lu). Values inside brackets are standard deviations (space group: monoclinic $P2_1/n$).

Atom	x	y	z	Occ.	U_{iso}	Site
(i) R = Sm						
Sm1	0.0	0.0	0.0	1.0	0.0044(5)	2*d*
Nb2	0.0	0.0	0.5	1.0	0.0049(8)	2*c*
Sr3	0.0096(7)	0.5374(3)	0.7522(6)	1.0	0.0071(4)	4*e*
O4	0.199(2)	0.330(2)	−0.037(3)	1.0	0.015(3)	4*e*
O5	0.398(2)	0.531(3)	0.2355(7)	1.0	0.015(3)	4*e*
O6	0.187(2)	0.283(2)	0.553(3)	1.0	0.015(3)	4*e*
(ii) R = Gd						
Gd1	0.0	0.0	0.0	1.0	0.001	2
Nb2	0.0	0.0	0.5	1.0	0.001	2
Sr3	0.0064(4)	0.53549(24)	0.75050(26)	1.0	0.002	4
O4	0.2209(13)	0.3059(14)	−0.0447(15)	1.0	0.005	4
O5	0.4134(15)	0.5269(19)	0.2353(4)	1.0	0.005	4
O6	0.1924(14)	0.2774(12)	0.5479(14)	1.0	0.005	4
(iii) R = Dy						
Dy1	0.0	0.0	0.0	1.0	0.01	2
Nb2	0.0	0.0	0.5	1.0	0.01	2
Sr3	0.0033(12)	0.53229(32)	0.7501(6)	1.0	0.01	4
O4	0.2275(27)	0.3018(27)	−0.040(4)	1.0	0.0233	4
O5	0.3826(25)	0.5042(30)	0.2339(8)	1.0	0.0233	4
O6	0.2106(31)	0.2612(30)	0.5417(35)	1.0	0.0233	4
(iv) R = Ho						
Ho1	0.0	0.0	0.0	1.0	0.001	2
Nb2	0.0	0.0	0.5	1.0	0.001	2
Sr3	0.0038(5)	0.52970(28)	0.75017(27)	1.0	0.002	4
O4	0.2201(14)	0.3062(15)	−0.0453(16)	1.0	0.005	4
O5	0.4114(16)	0.5316(21)	0.2356(4)	1.0	0.005	4
O6	0.1902(15)	0.2805(13)	0.5471(16)	1.0	0.005	4
(v) R = Y						
Y1	0.5	0.0	0.0	1.0	0.0102(9)	2
Nb2	0.0	0.5	0.0	1.0	0.0095(8)	2
Sr3	0.0073(4)	0.53247(16)	0.7499(6)	1.0	0.0139(3)	4
O4	0.2326(19)	0.2954(18)	−0.0281(19)	1.0	0.0093(15)	4
O5	0.4287(18)	0.5246(13)	0.2356(9)	1.0	0.0093(15)	4
O6	0.2011(21)	0.2688(19)	0.5495(18)	1.0	0.0093(15)	4
(Vi) R = Tm						
Tm1	0.5	0.0	0.0	1.0	0.0121(5)	2
Nb2	0.0	0.5	0.0	1.0	0.0070(6)	2
Sr3	0.0100(7)	0.53038(18)	0.7475(4)	1.0	0.0136(3)	4
O4	0.2339(20)	0.2968(20)	−0.0291(28)	1.0	0.024 (2)	4
O5	0.4249(22)	0.5128(16)	0.2347(7)	1.0	0.024 (2)	4
O6	0.1994(19)	0.2671(18)	0.5345(24)	1.0	0.024 (2)	4
(vii) R = Lu						
Lu1	0.5	0.0	0.0	1.0	0.0116(5)	2
Nb2	0.0	0.5	0.0	1.0	0.0056(6)	2
Sr3	0.0043(6)	0.5266(3)	0.7499(3)	1.0	0.0128(5)	4
O4	0.2225(21)	0.3013(19)	−0.0488(18)	1.0	0.01	4
O5	0.4112(16)	0.5177(24)	0.2376(4)	1.0	0.01	4
O6	0.1956(17)	0.2803(15)	0.5446(18)	1.0	0.01	4

the octahedral site. This decreasing volume is a result of the decrease in all the *a*, *b*, and c parameters.

The atomic coordinates, displacement parameters for the structures of Sr_2RNbO_6 are given in Table III. The trivalent lanthanides and pentavalent antimony are found to be fully ordered in the double-perovskite arrangement of alternating octahedra sharing corner oxygens. Our results show agreement with the observation by Karunadasa *et al*. (2003) in which the R^{3+} and Nb^{5+} are fully ordered in the double-perovskite structures, except for the R = Nd phase. The structure consists of corner-sharing alternate NbO_6 and RO_6 units in the form the zig-zag chains along the *c*-axis. Sr in general has a 12-coordination environment.

Table IV gives the bond distances of Sr–O, R–O, and Nb–O, and bond valence sum values (V_b) of the cation sites. From R = Sm to R = Lu, Nb atoms in the octahedral sites, the V_b values for the Nb sites are mostly <5.0 (except for R = Tm with a value of 5.17) and in general increases as the size of R^{3+} decreases. The <5.0 value indicates the sites are under tensile stress, or the cages too large. The V_b values for the Sr site in the Sr_2LnSbO_6 series are all around 2.0 (from 1.8 to 2.1). Note that V_b values for all R sites are significantly >3.0 (except for the R = Tm compound), representing a large compressive stress or overbonding for the R sites (cages too small).

In the monoclinic Sr_2RNbO_6 series, there are three R–O–Nb angles (R–O4–Nb, R–O5–Nb, and R–O6–Nb) that

https://doi.org/10.1017/S0885715618000593 Published online by Cambridge University Press

TABLE IV. Interatomic distances and bond valence sums (V_b) for Sr_2RNbO_6. Values inside brackets are standard deviations. The bond valence values, r_0 (Å) are 2.088 (Sm), 2.065 (Gd), 2.036 (Dy), 2.023 (Ho), 2.014 (Y), 2.000 (Tm), 1.971 (Lu), 2.118 (Sr), and 1.911 (Nb).

Atom	Atom		Distances	V_b
(i) R = Sm				
Sm1	O4	x2	2.297(7)	3.495
Sm1	O5	x2	2.283(7)	
Sm1	O6	x2	2.284(7)	
Nb2	O4	x2	2.050(7)	4.091
Nb2	O5	x2	2.051(7)	
Nb2	O6	x2	2.057(7)	
Sr3	O4		2.41(2)	2.056
Sr3	O4		3.02(2)	
Sr3	O4		2.78(3)	
Sr3	O5		2.423(14)	
Sr3	O5		2.644(15)	
Sr3	O5		3.438(14)	
Sr3	O6		2.468(15)	
Sr3	O6		2.81(2)	
Sr3	O6		2.98(3)	
(ii) R = Gd				
Gd1	O4	x2	2.251(4)	3.581
Gd1	O5	x2	2.256(4)	
Gd1	O6	x2	2.261(5)	
Nb2	O4	x2	2.025(5)	4.417
Nb2	O5	x2	2.023(3)	
Nb2	O6	x2	2.025(3)	
Sr3	O4		2.505(9)	1.888
Sr3	O4		2.832(13)	
Sr3	O4		2.933(13)	
Sr3	O5		2.480(9)	
Sr3	O5		3.406(9)	
Sr3	O5		3.370(11)	
Sr3	O5		2.645(11)	
Sr3	O6		2.518(9)	
Sr3	O6		2.812(12)	
Sr3	O6		2.944(13)	
(iii) R = Dy				
Dy1	O4	x2	2.237(8)	3.370
Dy1	O5	x2	2.298(8)	
Dy1	O6	x2	2.218(8)	
Nb2	O4	x2	1.993(8)	4.587
Nb2	O5	x2	2.049(8)	
Nb2	O6	x2	1.992(8)	
Sr3	O4		2.55 (2)	2.024
Sr3	O4		2.82 (3)	
Sr3	O4		2.92 (3)	
Sr3	O5		2.258(15)	
Sr3	O5		3.23 (2)	
Sr3	O5		2.81 (2)	
Sr3	O6		2.64 (2)	
Sr3	O6		2.74 (3)	
Sr3	O6		2.97 (3)	
Sr3	O6		3.42 (2)	
(iv) R = Ho				
Ho1	O4	x2	2.234(5)	3.326
Ho1	O5	x2	2.245(5)	
Ho1	O6	x2	2.245(5)	
Nb2	O4	x2	2.016(3)	4.509
Nb2	O5	x2	2.017(3)	
Nb2	O6	x2	2.017(3)	
Sr3	O4		2.474(10)	2.019
Sr3	O4		2.838(14)	
Sr3	O4		2.922(15)	
Sr3	O5		2.440(9)	
Sr3	O5		3.416(9)	
Sr3	O5		3.333(12)	
Sr3	O5		2.627(12)	
Sr3	O6		2.472(9)	
Sr3	O6		2.844(13)	
Sr3	O6		2.913(14)	
(v) R = Y				
Y1	O4	x2	2.208(7)	3.413
Y1	O5	x2	2.221(8)	
Y1	O6	x2	2.240(7)	
Nb2	O4	x2	1.975(7)	4.857
Nb2	O5	x2	1.991(7)	
Nb2	O6	x2	2.002(7)	
Sr3	O4		2.641(14)	1.802
Sr3	O4		2.830(14)	
Sr3	O4		2.869(14)	
Sr3	O4		3.385(14)	
Sr3	O5		2.557(11)	
Sr3	O5		3.294(11)	
Sr3	O5		3.297(8)	
Sr3	O5		2.637(8)	
Sr3	O6		2.527(12)	
Sr3	O6		2.74(2)	
Sr3	O6		2.98(2)	
(vi) R = Tm (237)				
Tm1	O4	x2	2.212(6)	3.308
Tm1	O5	x2	2.222(6)	
Tm1	O6	x2	2.227(6)	
Nb2	O4	x2	1.959(6)	5.182
Nb2	O5	x2	1.978(6)	
Nb2	O6	x2	1.959(6)	
Sr3	O4		2.63 (2)	1.786
Sr3	O4		2.80 (2)	
Sr3	O4		2.89 (2)	
Sr3	O4		3.37 (2)	
Sr3	O5		2.537(13)	
Sr3	O5		3.287(13)	
Sr3	O5		3.207(9)	
Sr3	O5		2.711(9)	
Sr3	O6		2.575(15)	
Sr3	O6		2.82 (2)	
Sr3	O6		2.87 (2)	
Sr3	O6		3.439(15)	
(vii) R = Lu				
Lu1	O4	x2	2.209(4)	3.159
Lu1	O5	x2	2.211(4)	
Lu1	O6	x2	2.205(4)	
Nb2	O4	x2	2.016(3)	4.518
Nb2	O5	x2	2.016(3)	
Nb2	O6	x2	2.016(3)	
Sr3	O4		2.452(10)	2.060
Sr3	O4		2.79(2)	
Sr3	O4		2.95(2)	
Sr3	O5		2.418(10)	
Sr3	O5		3.390(9)	
Sr3	O5		3.209(14)	
Sr3	O5		2.704(14)	
Sr3	O6		2.471(10)	
Sr3	O6		2.83(2)	
Sr3	O6		2.90(2)	

are between different NbO_6 and RO_6 octahedral units (Table V). While the R–O6–Nb angle is a measure for the deviation from the ideal value of 180° along the c-axis, the R–O4–Nb and R–O5–Nb angle bending are related to the rotation of the octahedra with respect to the ab plane (Figures 3 and 4). These R–O–Nb angles all deviate rather

https://doi.org/10.1017/S0885715618000593 Published online by Cambridge University Press

TABLE V. Selected bond angles (°) for Sr_2RNbO_6. Values inside brackets are standard deviations.

	O–*R*–O				O–Nb–O				*R*–O–Nb		
R	O4–*R*–O4 O5–*R*–O5 O6–*R*–O6	O4–*R*–O6	O4–*R*–O5	O5–*R*–O6	O4–Nb–O4	O4–Nb–O6	O4–Nb–O5	O5–Nb–O6	*R*–O4–Nb	*R*–O6–Nb	*R*–O5–Nb
Sm	180.0	92.6(7)	94.0(6)	91.5(7)	180.0	94.8(8)	93.6(9)	91.3(7)	146.8(8)	147.5(8)	146.6(7)
Gd	180.0	90.9(4)	91.3(4)	92.1(4)	180.0	91.3(4)	91.0(5)	90.8(4)	152.3(5)	151.2(5)	151.3(4)
Dy	180.0	91.6(8)	92.3(8)	93.9(9)	180.0	93.9(9)	95.8(10)	93.0(9)	155.2(11)	157.9(12)	143.3(7)
Ho	180.0	91.6(4)	92.0(4)	91.9(4)	180.0	91.0(4)	91.3(5)	91.8(5)	151.9(5)	150.7(5)	150.2(5)
Y	180.0	91.1(6)	93.5(5)	94.3(5)	180.0	90.3(7)	90.4(6)	91.1(5)	160.8(8)	152.9(6)	155.9(6)
Tm	180.0	90.7(6)	92.6(7)	90.4(6)	180.0	90.0(6)	91.5(8)	91.2(7)	160.5(8)	158.0(8)	155.6(7)
Lu	180.0	92.1(5)	90.3(5)	90.2(5)	180.0	91.1(6)	90.9(6)	90.6(5)	151.8(5)	152.3(5)	151.3(5)

significantly from 180° (approximately between 147 and 161°). The *R*–O4–Nb angles range from 146 to 161°; the *R*–O5–Nb angles range from 148 to 158°; *R*–O6–Nb angles range from 147 to 156°. One also notes that the *R* and Nb sites in the NbO_6 and RO_6 octahedra also have distorted environment, as evidenced from different *R*–O and Nb–O distances (Table IV), and different O–*R*–O and O–Nb–O bond angles (Table V). While the O4–*R*–O4 and O4–Nb–O4 angles are 180°, the remaining O–*R*–O and O–Nb–O angles all deviate from 90°.

A. Reference X-ray diffraction pattern

The powder X-ray diffraction pattern of Sr_2DyNbO_6 is given in Table VI as an example. In this pattern, the symbols "*M*" and "+" refer to peaks containing contributions from two and more than two reflections, respectively. The peak that has the strongest intensity in the entire pattern is assigned an intensity of 999 and other lines are scaled relative to this value. In general, the *d*-spacing values are calculated values from refined lattice parameters. The intensity values reported are integrated intensities (rather than peak heights) based on the

TABLE VI. X-ray powder pattern for Sr_2DyNbO_6, $P2_1/n$, $a = 5.81448(10)$ Å, $b = 5.87239(10)$ Å, $c = 8.2534(2)$ Å, $\beta = 90.154(2)°$. The symbols "*M*" and "+" refer to peaks containing contributions from two and more than two reflections, respectively.

d	*I*	*h*	*k*	*l*	*d*	*I*	*h*	*k*	*l*	*d*	*I*	*h*	*k*	*L*
4.7848	7	0	1	1	4.7543	10	1	0	−1*M*	4.7543	10	1	0	1*M*
4.1302	91	1	1	0*M*	4.1302	91	0	0	2*M*	3.6949	18	1	1	−1*M*
3.6949	18	1	1	1*M*	2.9362	283	0	2	0	2.9200	999	1	1	−2*M*
2.9200	999*	1	1	2*M*	2.9072	217	2	0	0	2.7664	27	0	2	1
2.4989	7	1	2	−1	2.4856	18	2	1	−1*M*	2.4856	18	1	0	3*M*
2.0651	376	2	2	0*M*	2.0651	376	0	0	4*M*	2.0055	21	0	2	3+
1.8552	10	1	3	0	1.8472	26	2	2	2+	1.8405	6	1	1	4*M*
1.8405	6	3	1	0*M*	1.8099	11	1	3	−1*M*	1.8099	11	1	3	1*M*
1.6920	134	1	3	−2*M*	1.6920	134	1	3	2*M*	1.6882	153	0	2	4
1.6832	190	2	0	−4*M*	1.6832	190	3	1	−2*M*	1.6796	154	2	0	4*M*
1.6796	154	3	2	2*M*	1.6535	6	2	2	−3	1.4681	32	0	4	0
1.4613	65	2	2	−4	1.4585	52	2	2	4	1.4536	37	4	0	0
1.4454	5	0	4	1	1.3790	5	1	3	4	1.3105	20	2	4	0
1.3072	31	3	3	−2	1.3058	61	1	1	−6*M*	1.3058	61	3	3	2*M*
1.3044	36	1	1	6	1.3027	38	4	2	0	1.1962	24	0	4	4
1.1898	11	4	0	−4	1.1868	15	4	0	4	1.1837	5	2	4	−3
1.1826	5	2	4	3	1.1403	5	1	5	−1	1.1089	23	1	5	−2*M*
1.1089	23	1	5	2*M*	1.1068	17	2	4	−4	1.1055	29	2	4	4*M*
1.1055	29	1	3	−6*M*	1.1045	16	1	3	6	1.1030	35	3	1	−6*M*
1.1030	35	4	2	−4*M*	1.1004	51	5	1	−2+	1.0988	20	5	1	2
1.0329	27	4	4	0	1.0317	11	0	0	8	0.9763	16	3	5	−2
0.9756	14	3	5	2	0.9742	18	3	5	−6	0.9732	32	0	2	8*M*
0.9732	32	2	0	−8*M*	0.9722	37	3	3	6*M*	0.9722	37	5	3	−2*M*
0.9712	35	2	0	8*M*	0.9712	35	5	3	2*M*	0.9691	13	6	0	0
0.9276	5	2	6	0	0.9244	16	4	4	−4	0.9237	19	2	2	−8
0.9230	14	4	4	4	0.9223	14	2	2	8	0.9202	16	6	2	0
0.8829	13	1	5	−6*M*	0.8829	13	1	5	6*M*	0.8792	15	5	1	−6
0.8781	7	6	0	−4	0.8770	12	5	1	6	0.8762	7	6	0	4
0.8460	14	2	6	−4*M*	0.8460	14	2	6	4*M*	0.8441	15	0	4	8
0.8424	10	4	0	−8	0.8412	21	6	2	−4	0.8402	8	4	0	8
0.8397	23	6	2	4	0.8303	7	1	7	0	0.8261	14	1	7	−1*M*
0.8261	14	1	7	1*M*	0.8239	5	1	5	−7					

The symbol * indicates the particular peak has the strongest intensity of the entire pattern and is designated a value of "999".

https://doi.org/10.1017/S0885715618000593 Published online by Cambridge University Press

corresponding profile parameters. For resolved overlapped peaks, intensity-weighted calculated *d*-spacing, along with the observed integrated intensity and the *hkl* indices of both peaks (for "*M*"), or the *hkl* indices of the strongest peak (for "+") are used. For peaks that are not resolved at the instrumental resolution, the intensity-weighted average *d*-spacing and the summed integrated intensity value are used. In the case of a cluster, unconstrained profile fits often reveal the presence of multiple peaks, even when they are closer than the instrumental resolution. In this situation, both *d*-spacing and intensity values are reported independently. The reference patterns for Sr_2RNbO_6 have been submitted for inclusion in the PDF: Sr_2SmNbO_6 (00-063-0698); Sr_2GdNbO_6 (00-062-0323); Sr_2DyNbO_6 (00-062-0325); Sr_2HoNbO_6 (00-062-0324); Sr_2YNbO_6 (00-062-0297); Sr_2TmNbO_6 (00-062-0326); Sr_2LuNbO_6 (00-062-0300).

IV. SUMMARY

Crystal structure and reference patterns of the double perovskites Sr_2RNbO_6 (R = Sm, Gd, Dy, Ho, Y, Tm, and Lu) series have been determined and published as part of the PDF. Among the series, the literature reported that the phase of R = La (cubic) and R = Pr (cubic) is different from the rest of the lanthanide members with smaller size of R. Sr_2RNbO_6 (R = Sm, Gd, Dy, Ho, Y, Tm, and Lu) adopt the monoclinic $P2_1/n$ space group. The structure consists of corner-sharing alternate NbO_6 and RO_6 units in the form of the zig-zag chains along the *c*-axis. Sr in general has a 12-coordination environment. The deviation from ideal perovskite geometry has been discussed. Bond valence sum calculations indicated that all Nb adopt 5+ valence state in these compounds, except with large tensile stress (V_b values mostly <5 except for the R = Tm member). Compressive stress has been found at the R^{3+} site throughout the series (V_b ranges from 3.2 to 3.6).

SUPPLEMENTARY MATERIAL

The supplementary material for this article can be found at https://doi.org/10.1017/S0885715618000593

ACKNOWLEDGEMENTS

Use of the Advanced Photon Source at Argonne National Laboratory was supported by the US Department of Energy, Office of Science, Office of Basic Energy Sciences, under Contract No. DE-AC02-06CH11357. The authors acknowledge the partial financial support from the ICDD Grants-in-Aid Program.

Brese, N. E. and O'Keeffe, M. (**1991**). "Bond-valence parameters for solids," Acta Crystallogr. B **47**, 192–197.

Brown, I. D. and Altermatt, D. (**1985**). "Bond-valence parameters obtained from a systematic analysis of the Inorganic Crystal Structure Database," Acta Crystallogr. B **41**, 244–247.

Chan, J. C., Bock, J. A., Guo, H., Trolier-McKinstry, S., and Randall, C. A. (**2017**). "High-temperature thermoelectric characterization of filled strontium barium niobates: power factors and carrier concentrations," Mater. Res. **32**, 1160–1167.

Dalesio, L. R., Hill, J. O., Kraimer, M., Lewis, S., Murray, D., Hunt, S., Watson, W., Clausen, M., and Dalesio, J. (**1994**). "Nuclear instruments & methods in physics research section A – accelerators spectrometers detectors and associated equipment," **352**, 179–184.

Grebille, D., Lambert, S., Bouree, F., and Petricek, V. (**2004**). "Contribution of powder diffraction for structure refinements of aperiodic misfit cobalt oxides," J. Appl. Crystallogr. **37**, 823–831.

Henmi, K. and Hinatsu, Y. (**1999**). "Crystal structures and magnetic properties of ordered perovskites Ba_2LnNbO_6 (Ln = Lanthanide elements)," J. Solid State Chem. **148**, 353–360.

Huang, Z., Yan, D., Tien, T., and Chen, I. (**1991**). "Phase relationships in the La_2O_3-SrO-Nb_2O_5 system," Mater. Lett. **11**, 286–290.

Karunadasa, H., Huang, Q., Ueland, B. G., Schiffer, P., and Cava, R. J. (**2003**). "Ba_2LnSbo_6 and Sr_2LnSbO_6 (Ln = Dy, Ho, Gd) double perovskites: lanthanides in the geometrically frustrating fcc lattice," PNAS **100**, 8097–8102.

Larson, A. C. and von Dreele, R. B. (**2004**). General Structure Analysis System (GSAS), Los Alamos National Laboratory Report LAUR 86-748, Los Alamos, USA.

Lee, P. L., Shu, D., Ramanathan, M., Preissner, C., Wang, J., Beno, M. A., Von Dreele, R. B., Ribaud, L., Kurtz, C., Antao, S. M., Jiao, X., and Toby, B. H. (**2008**). "A twelve-analyzer detector system for high-resolution powder diffraction," J. Synchrotron Radiat. **15**, 427–432.

Li, S., Funahashi, R., Matsubara, I., Yamada, H., Ueno, K., and Sodeoka, S. (**2001**). "Synthesis and thermoelectric properties of the new oxide ceramics $Ca_{3-x}Sr_xCo_4O_{9+\delta}$ (x = 0.0–1.0)," Ceram. Int. **27**, 321–324.

Masset, A. C., Michel, C., Maignan, A., Hervieu, M., Toulemonde, O., Studer, F., and Raveau, B. (**2000**). "Misfit-layered cobaltite with an anisotropic giant magnetoresistance: $Ca_3Co_4O_9$," Phys. Rev. B **62**, 166–175.

Maupoey, Z., Azcondo, M. T., Amador, U., Kuhn, A., Perez Flores, J. C., De Paz, J. R., Bonanos, N., and Garcia Alvarado, F. (**2012**). "The role of the Eu^{3+}/Eu^{2+} redox-pair in the electrical properties of $Sr_2EuNb_{1-x}Ti_xO_{6-d}$ oxides," J. Mater. Chem. **22**, 18033–18042.

McMurdie, H., Morris, M., Evans, E., Paretzkin, B., Wong-Ng, W., Ettlinger, L., and Hubbard, C. R. (**1986**) "JCPDS – International Centre for Diffraction Data task group on cell parameter refinement," Powder Diffr. **1**, 66–76.

Minami, H., Itaka, K., Kawaji, H., Wang, Q. J., Koinuma, H., and Lippmaa, M. (**2002**). "Rapid synthesis and characterization of $(Ca_{1-x}Ba_x)_3Co_4O_9$ thin films using combinatorial methods," Appl. Surf. Sci. **197**, 442–447.

Moon, Ji-W., Masuda, Y., Seo, W-S., and Koumoto, K. (**2001**). "Influence of ionic size of rare-earth of rare-earth site on the thermoelectric properties of $RCoO_3$-type perovskite cobalt oxides," Mater. Sci. Eng. **B85**, 70–75.

Nolas, G. S., Sharp, J., and Goldsmid, H. J. (**2001**). *Thermoelectric: Basic Principles and New Materials Developments* (Springer, New York).

Otani, M., Lowhorn, N. D., Schenck, P. K., Wong-Ng, W., and Green, M. (**2007**). "A high-throughput thermoelectric screening tool for rapid construction of thermoelectric phase diagrams," Appl. Phys. Lett. **91**, 132102.

PDF, Powder Diffraction File (**2018**). Produced by International Centre for Diffraction Data, 12 Campus Blvd., Newtown Squares, PA. 19073-3273, USA.

Rietveld, H. M. (**1969**). "A profile refinement method for nuclear and magnetic structures," J. Appl. Crystallogr. **2**, 65–71.

Sehlin, S. R., Anderson, H. U., and Sparlin, D. M. (**1995**). "Semi-empirical model for the electrical properties of $La_{1-x}Ca_xCoO_3$," Phys. Rev. B **52**, 11681.

Shannon, R. D. (**1976**). "Revised effective ionic radii and systematic studies of interatomic distances in halides and chalcogenides," Acta Crystallogr. **A32**, 751–767.

Terasaki, I., Sasago, Y., and Uchinokura, K. (**1997**). "Large thermoelectric power in $NaCo_2O_4$ single crystals", Phys. Rev. B **56**, 12685–12687.

Trunov, V. K., Sirotinkin, V. P., and Evdokimov, A. A. (**1983**). "An X-ray diffraction study of the compounds Sr_2LnEO_6 (E = Nb or Ta)," Russ. J. Inorg. Chem. (Engl. Transl.) **28**, 349.

Wang, J., Toby, B. H., Lee, P. L., Ribaud, L., Antao, S., Kurtz, C., Ramanathan, M., Von Dreele, R. B., and Beno, M. A. (**2008**). "A dedicated powder diffraction beamline at the Advanced Photon Source: commissioning and early operational results," Rev. Sci. Instrum. **79**, 085105.

https://doi.org/10.1017/S0885715618000593 Published online by Cambridge University Press

Wang, S., Venimadhav, A., Guo, S., Chen, K., Li, Q., Soukiassian, A., Schlom, D. G., Pan, X. Q., Wong-Ng, W., Vaudin, M. D., Cahill, D. G., and Xi, X. X. (**2009**). "Structural and thermoelectric properties of $Bi_2Sr_2Co_2O_y$ thin films on $LaAlO_3$ (100) and fused silica substrates," Appl. Phys. Lett. **94**, 022110.

Wang, Y., Sui, Y., Ren, P., Wang, L., Wang, X., Su, W., and And Fan, H. J. (**2010**). "Correlation between the structural distortions and thermoelectric characteristics in $La_{1-x}A_xCoO_3$ (A = Ca and Sr)," Inorg. Chem. **49**, 3216–3223.

Wong-Ng, W., McMurdie, H. F., Hubbard, C. R., and Mighell, A. D. (**2001**). "JCPDS-ICDD Research Associateship (Cooperative Program with NBS/NIST)," J. Res. Natl. Inst. Stand. Technol. **106**, 1013–1028.

Wong-Ng, W., Hu, Y. F., Vaudin, M. D., He, B., Otani, M., Lowhorn, N. D., and Li, Q. (**2007**). "Texture analysis of a $Ca_3Co_4O_9$ thermoelectric film on Si (100) substrate," J. Appl. Phys. **102**, 33520.

Wong-Ng, W., Liu, G., Martin, J., Thomas, E., Lowhorn, N., and Otani, M. (**2010**). "Phase compatibility of the thermoelectric compounds in the Sr-Ca-Co-O system," J. Appl. Phys. **107**, 033508.

Wong-Ng, W., Yan, Y., Kaduk, J. A., and Tang, X. F. (**2016**). "X-ray powder diffraction reference patterns for $Bi_{1-x}Pb_xOCuSe$," Powder Diffr. **31**, 223–228.

Wong-Ng, W., Yan, Y., Kaduk, J. A., and Tang, X. F. (**2017**). "Crystallographic and powder diffraction reference patterns for thermoelectric oxyselenides $Bi_{1-x}A_xOCuSe$ (A = alkaline-earth elements)," Solid State Sci. **72**, 55–63.

https://doi.org/10.1017/S0885715618000593 Published online by Cambridge University Press